

# Invaded cluster simulations of the $XY$ model in two and three dimensions

I. Dukovski and J. Machta\*

*Department of Physics, University of Massachusetts,  
Amherst, Massachusetts 01003-3720*

L. V. Chayes†

*Department of Mathematics, University of California,  
Los Angeles, California 90095-1555*

(Dated: November 6, 2018)

## Abstract

The invaded cluster algorithm is used to study the  $XY$  model in two and three dimensions up to sizes  $2000^2$  and  $120^3$  respectively. A soft spin  $O(2)$  model, in the same universality class as the three-dimensional  $XY$  model, is also studied. The static critical properties of the model and the dynamical properties of the algorithm are reported. The results are  $K_c = 0.45412(2)$  for the three-dimensional  $XY$  model and  $\eta = 0.037(2)$  for the three-dimensional  $XY$  universality class. For the two-dimensional  $XY$  model the results are  $K_c = 1.120(1)$  and  $\eta = 0.251(5)$ . The invaded cluster algorithm does not show any critical slowing for the magnetization or critical temperature estimator for the two-dimensional or three-dimensional  $XY$  models.

---

\*Electronic address: machta@physics.umass.edu

†Electronic address: lchayes@math.ucla.edu

## I. INTRODUCTION

In this paper we present a Monte Carlo study of the  $XY$  model using the invaded cluster (IC) algorithm. The purpose of this study is both to obtain high precision results for the  $XY$  model and to test the efficacy of the invaded cluster method for phase transitions with continuous symmetry breaking. The  $XY$  model is in the  $O(2)$  universality class and in two dimensions the transition is of the Kosterlitz-Thouless type [1]. Theoretical and computational studies of the  $O(2)$  critical point include high temperature series expansions [2], renormalization-group calculations [3] and Monte Carlo (MC) simulations [4, 5, 6, 7]. The  $\lambda$  transition in  $^4\text{He}$  is also in the  $O(2)$  universality class and the specific heat exponent  $\alpha$  for this system has been measured to very high precision [8, 9, 10].

Recent Monte Carlo studies of the  $XY$  transition use versions of the Wolff algorithm [11] because near the critical point they are much more efficient than local algorithms. The Wolff algorithm is an example of a cluster algorithm of the kind first introduced by Swendsen and Wang [12, 13] for Ising-Potts models. The central idea of cluster algorithms is to identify clusters of sites by a bond percolation process correlated to the spin configuration. The spins of each cluster are then independently flipped. Cluster algorithms can be extremely efficient when the percolation process that defines the clusters has a percolation threshold that coincides with the phase transition of the spins. This situation holds for the original Swendsen-Wang algorithm applied to Ising-Potts models and was later shown to hold for a variety of other spin systems with discrete symmetries [14, 15, 16]. Wolff [11] showed how to extend cluster algorithms to spin models with  $O(n)$ -symmetry by an Ising embedding method.

Invaded cluster (IC) algorithms [17, 18, 19] are cluster algorithms with the property that they find and simulate the critical point automatically without *a priori* knowledge of the critical temperature. The critical temperature is a direct output of the algorithm and the magnetic exponents can be obtained from finite-size scaling of the cluster size distribution. In addition to providing the critical temperature and magnetic exponent without having to invoke methods such as histogram re-weighting, IC algorithms appear to have less critical slowing than corresponding Swendsen-Wang or Wolff algorithms [19]. IC algorithms can, in principle, be constructed whenever a conventional cluster algorithm is available with the property that the bond percolation process has a percolation threshold that coincides with

the phase transition. IC algorithms have thus far been applied to systems with discrete symmetry breaking including Ising-Potts [17, 18, 20, 21] models, Widom-Rowlinson models [22] and the fully frustrated Ising model [21]. In this paper we show how Wolff's embedding scheme can be used to construct an efficient IC algorithm for simulating the  $O(2)$  critical point in three dimensions and the Kosterlitz-Thouless point in two dimensions.

One of our objectives is to obtain a high precision value of the  $\eta$  exponent for the  $O(2)$  universality class. Because  $\eta$  is itself very small, it has proved difficult to measure it with much precision. One of the difficulties is the presence of corrections to scaling. Recently, Hasenbusch and Török [6, 7] proposed a method to minimize this difficulty by considering a soft spin  $O(2)$  model with a parameter controlling the variance in the length of the spin vectors. By adjusting this parameter they minimize corrections to scaling and improve their estimate of  $\eta$ . Below we apply a modified version of the IC algorithm to the soft spin model.

In the next Section we describe the IC algorithm for the  $XY$  model. In Sec. III we give results for the critical temperature, magnetic exponents and dynamic properties of the  $XY$  model in two and three dimensions. In Sec. IV we describe the algorithm and present results for the soft spin model. Conclusions are presented in Sec. V.

## II. INVADDED CLUSTER ALGORITHM FOR THE $XY$ MODEL

The algorithms for the  $XY$  model used in this paper are obtained by combining the invaded cluster method and Wolff's embedding scheme for continuous spin models. The  $XY$  model is defined by the Hamiltonian:

$$\beta H = -K \sum_{\langle i,j \rangle} \vec{s}_i \cdot \vec{s}_j \quad (1)$$

where  $\vec{s}_i$  is a two dimensional unit vector and the summation is over all nearest neighbor bonds on the lattice, here either the square or cubic lattice with periodic boundary conditions.

We begin by describing a version of Wolff's algorithm for the  $XY$  model. On each Monte Carlo step we choose a two-dimensional unit vector  $\vec{r}$ . For each bond  $(i, j)$  of the lattice, the bond is called *satisfied* if both spins lie on the same side of the line perpendicular to the unit vector, that is,

$$(\vec{s}_i \cdot \vec{r})(\vec{s}_j \cdot \vec{r}) > 0. \quad (2)$$

Satisfied bonds are then *occupied* with probability

$$P(\vec{s}_i, \vec{s}_j) = 1 - \exp[-2K(\vec{r} \cdot \vec{s}_i)(\vec{r} \cdot \vec{s}_j)]. \quad (3)$$

One way to implement the occupation of bonds with this probability is to independently assign random numbers  $u_{i,j}$ , uniformly chosen from the interval  $[0, 1)$  to every bond of the lattice and then to occupy the satisfied bonds if  $u_{i,j} < P(\vec{s}_i, \vec{s}_j)$ . An equivalent approach, which provides a useful link to the IC methodology, is to define  $\kappa_{i,j}$  from  $u_{i,j}$  by substituting  $u_{i,j}$  for  $P(\vec{s}_i, \vec{s}_j)$  and  $\kappa_{i,j}$  for  $K$  in Eq. (3) and then solving for  $\kappa_{i,j}$ ,

$$\kappa_{i,j} = -\log(1 - u_{i,j}) / (2(\vec{r} \cdot \vec{s}_i)(\vec{r} \cdot \vec{s}_j)). \quad (4)$$

Satisfied bonds with  $\kappa_{i,j} < K$  are occupied. The occupied bonds define a set of connected clusters. Single sites with no occupied bonds are considered clusters so that every lattice site is uniquely a member of some cluster.

Once the clusters are identified each cluster is *flipped* with probability 1/2. A cluster is flipped by reflecting every spin in the cluster through the line perpendicular to  $\vec{r}$ ,

$$\vec{s}_i \rightarrow R(\vec{r})\vec{s}_i \quad (5)$$

where

$$R(\vec{r})\vec{s}_i = \vec{s}_i - 2(\vec{s}_i \cdot \vec{r})\vec{r}. \quad (6)$$

Flipping clusters with probability one half yields a new spin configurations and completes one MC step. It is straightforward to show that the algorithm is ergodic and satisfies detailed balance.

Wolff's original paper [11] introduces two innovations. The first is to grow and flip only a single cluster in each Monte Carlo step. The second is the generalization of cluster methods to spin models with continuous symmetries. Only the generalization to continuous symmetries is used here and combined with the invaded cluster methodology. In fact, Wolff's single cluster method is not compatible with the invaded cluster methodology. When we speak of the Wolff algorithm in the following we mean the algorithm described above for which all clusters are defined and flipped in a single MC step.

Cluster algorithms can generally be viewed as a sequence of bond moves and spin moves. During the bond move a configuration of occupied bonds and the associated set of clusters are generated from the spin configuration. This is done by occupying satisfied bonds with a

probability that depends on the simulation temperature. During the spin move a new spin configuration is obtained by randomly flipping clusters. The bond configurations can be viewed as a correlated percolation model. For a cluster algorithm to be efficient, the correlated percolation model should have a percolation transition that coincides with the critical point of the spin model. If this holds then clusters of all sizes are flipped during a single MC step and changes to the spin configuration occur on all length scales. For Ising-Potts models the correlated percolation model associated with the Swendsen-Wang algorithm is the Fortuin-Kastelyn random cluster model and the equivalence of the percolation threshold and the critical point is well-understood [23, 24]. The percolation properties of the bonds defined by the Wolff algorithm for the  $XY$  model have recently been investigated [25]. The conclusion is the same as for the Ising-Potts models: the critical point for the three-dimensional  $XY$  model and Kosterlitz-Thouless point for the two-dimensional  $XY$  model coincide with the percolation threshold for the bonds defined by the Wolff algorithm.

The invaded cluster methodology relies on the equivalence of the phase transition in the spin model and the percolation transition of the occupied bonds to find and simulate the phase transition without prior knowledge of the critical coupling. Like other cluster algorithms, a full MC step consists of a bond move followed by a spin move. The spin move is the same as for standard cluster algorithms but the bond moves differs. In the IC bond move, satisfied bonds are occupied one at a time in random order until a signature of percolation is first observed. The set of occupied bonds obtained in this way defines bond clusters and these are flipped in the usual way. The signature of percolation is incorporated in a stopping condition that is tested after each new bond is occupied. In this paper we use a topological stopping condition, which requires that at least one cluster wraps around the lattice in at least one direction.

For the most part, the IC algorithm closely parallels the Wolff algorithm. First a unit vector is randomly chosen and satisfied bonds are determined with respect to this unit vector as described in the paragraph including Eq. (2). Then uniform random numbers,  $u_{i,j}$  are assigned to each bond and non-uniform random numbers,  $\kappa_{i,j}$  are obtained from them according to Eq. (4). The next step of the IC algorithm differs from the Wolff algorithm. Satisfied bonds are occupied *one at a time* according to the ordering defined by  $\kappa_{i,j}$  with the satisfied bond having the smallest value of  $\kappa$  occupied first. After each bond is occupied, the set of clusters is updated and the stopping condition is checked. If no cluster wraps around

the lattice the satisfied bond with the next largest  $\kappa$  is occupied but if some cluster wraps around the lattice in some direction the bond move is completed and no further bonds are occupied. The largest value of  $\kappa$  chosen during the bond move is called  $\tilde{\kappa}$ . The spin move is identical to the Wolff algorithm: with probability 1/2, each cluster is reflected through the line perpendicular to  $\vec{r}$  according to Eqs. (5) and (6).

The IC algorithm simulates the critical point and  $\tilde{\kappa}$  is an estimator of the critical coupling. To see why this is the case, consider a large system with a spin configuration that is typical of the critical point. The correlated percolation threshold for the occupied bonds is related to critical coupling according to Eq. (3). That is, if satisfied bonds are occupied with probability  $P_c(\vec{s}_i, \vec{s}_j) = 1 - \exp[-2K_c(\vec{r} \cdot \vec{s}_i)(\vec{r} \cdot \vec{s}_j)]$ , the occupied bonds will just percolate [25]. Occupying bonds with probability  $P_c(\vec{s}_i, \vec{s}_j)$  is the same as occupying all satisfied bonds one at a time in ascending order of  $\kappa$  and stopping at the largest  $\kappa$  such that  $\kappa \leq K_c$ . The IC algorithm works in the same way except that satisfied bonds are added until a cluster wraps around the system. For a large system, this event will occur with  $\tilde{\kappa}$  nearly equal to  $K_c$ . Thus, if the system is at criticality, a single step of the IC algorithm is almost identical to a single step of the Wolff algorithm at  $K_c$  and  $\tilde{\kappa} \approx K_c$ . So long as the fluctuations in  $\tilde{\kappa}$  become small as the system size increase, the IC algorithm and the Wolff algorithm at  $K_c$  will sample the same state in the thermodynamic limit. However, in finite volume, the invaded cluster algorithm defines an ensemble that is different than the canonical ensemble and has different finite-size scaling properties.

So far we have assumed the spin system is already at the critical point. Suppose that the spin configuration is typical of the low temperature phase, then there will be more satisfied bonds than at criticality and a smaller fraction will be needed to form a spanning cluster so that  $\tilde{\kappa} < K_c$ . The invaded cluster MC step thus corresponds to a Wolff MC step at temperature  $T = J/\tilde{\kappa} > T_c$  so that the system is warmed. A similar argument shows that if the system starts in the high temperature phase, it is cooled by the IC algorithm so that there is negative feedback mechanism that forces the system to the critical point independent of the starting configuration. A detailed discussion of these arguments in the context of Ising-Potts models is given in Ref. [18].

For the 2D  $XY$  model, the IC algorithm described above does not perform well. The problem is similar to a problem that occurs in the 2D Ising model. Specifically, at criticality, the satisfied bonds themselves just percolate. This means that in a significant fraction of

spin configurations, spanning is not possible. It also means that the distribution of the temperature estimator is broad because of spin configurations for which spanning is just barely possible. The problem is even worse for the the  $XY$  model. Since the unit vector  $\vec{r}$  is randomized from one step to the next, spanning on one Monte Carlo step does not guarantee spanning on the next Monte Carlo step as it does in the Ising case. As a result, a small fraction of the time, no spanning cluster can be found for the chosen unit vector  $\vec{r}$ . Furthermore, the distribution of the temperature estimator is very broad because some spin configurations and unit vectors just barely allow spanning yielding a very small value of the temperature estimator.

These problems can be alleviated by taking advantage of a second independent set of satisfied bonds. Let's refer to the bonds that are satisfied with respect to the definition of Eq. (2) as *red* satisfied bonds. Let  $\vec{b}$  be a unit vector perpendicular to  $\vec{r}$  and define bond  $(i, j)$  as *blue* satisfied if

$$(\vec{s}_i \cdot \vec{b})(\vec{s}_j \cdot \vec{b}) > 0. \quad (7)$$

To increase the probability that we obtain a spanning cluster, we can occupy both red and blue satisfied bonds. Two values of  $\kappa$ , one with respect to  $\vec{r}$  and the other with respect to  $\vec{b}$ , are assigned to each bond using Eq. (4) and a single value of  $u$ . The entire set of  $\kappa$ 's, for both red and blue satisfied bonds, is ordered. Bond are either red or blue occupied in the order prescribed by the  $\kappa$ 's and sets of red and blue clusters are identified and updated after each new bond is occupied. The first cluster to span, either red or blue, stops the process of occupying bonds. During the spin move, both sets of clusters are flipped with probability 1/2 according to Eqs. (5) and (6) with  $\vec{r}$  replaced by  $\vec{b}$  for the blue clusters. One way of looking at this algorithm is that it utilizes two independent embeddings of the Ising model in the  $XY$  model, one embedding relative to  $\vec{r}$  and the other relative to  $\vec{b}$ . The two embedding method was always able to find a spanning cluster and it produces a less broad distribution for the temperature estimator. Nonetheless, the distribution of  $\tilde{\kappa}$  is still very broad and we find better statistics by averaging  $1/\tilde{\kappa}$ . All results reported for the two-dimensional  $XY$  model use the two-embedding method.

### III. RESULTS

The algorithm was implemented on systems with maximum linear size  $L = 120$  for three dimensions and  $L = 2000$  for two dimensions. Each run consisted of 160000 MC steps for three dimensions and 10000 MC steps for two dimensions. We collected statistics for the estimator of the critical coupling,  $\tilde{\kappa}$  and the size of the spanning cluster,  $M$ . For the two-dimensional model we obtained the estimator of critical coupling as inverse of the estimator of the critical temperature. The average critical coupling and its error bars were obtained using the blocking method [13] with 100 blocks of 100 data points each for two dimensions and 160 blocks of 1000 data points each for three dimensions. The average size of the spanning cluster and its error bars was obtained using the bootstrap method [13]. The reported error bars are one standard deviation. The simulation time was  $10^{-5}$  CPU seconds per spin per MC sweep on a 450MHz Pentium III machine running Linux.

#### A. Critical temperature of the three-dimensional XY model

Figure 1 shows the average value of  $\tilde{\kappa}$  for the three-dimensional XY model versus the inverse of the linear size of the system  $1/L$ . We fit the data for  $L \geq 10$  to a function of the form:

$$\langle \tilde{\kappa}(L) \rangle = \frac{K_c}{1 + aL^{-p}} \quad (8)$$

where  $K_c$ ,  $a$  and  $p$  are parameters of the fit. The results of the fit are  $K_c = 0.45412(2)$ ,  $a = -0.64(2)$  and  $p = 1.211(9)$  with  $\chi^2 = 6.23$ ,  $\chi^2/d.o.f. = 0.69$  and the confidence level is  $Q = 0.72$ . The value for the critical coupling  $K_c$  compares well with values used in the literature as shown in Table VI. Note that  $p \neq 1/\nu \approx 1.5$  as would be expected from naive finite size scaling arguments. As is the case for Ising-Potts systems, the IC ensemble for the XY model does not have the same finite size scaling properties as the canonical ensemble.

The validity of the IC method is justified by the fact that the width of the distribution of  $\tilde{\kappa}$  decreases as  $L$  increases. Figure 2 shows the standard deviation  $\sigma_{\tilde{\kappa}}$  of  $\tilde{\kappa}$  as a function of  $1/L$  and suggests that

$$\lim_{L \rightarrow \infty} \sigma_{\tilde{\kappa}} = 0 \quad (9)$$

and therefore we expect a sharp distribution of  $\tilde{\kappa}$  for  $L = \infty$ . The solid curve in Fig. 2 is the result of a fit to the data for  $L \geq 50$  to the functional form  $\sigma_{\tilde{\kappa}} = a + bL^{-q}$  yielding



$a = 0.0002(10)$ ,  $b = 0.43(3)$  and  $q = 0.66(3)$ .

### B. Kosterlitz-Thouless temperature

Figure 3 shows  $\langle 1/\tilde{\kappa}(L) \rangle^{-1}$  as a function of  $1/\log(L)$  for the two-dimensional  $XY$  model. We fit the data for  $L \geq 160$  to the function,

$$\langle 1/\tilde{\kappa}(L) \rangle^{-1} = \frac{K_c}{1 + a(\log(L))^{-2}} \quad (10)$$

where  $K_c$  and  $a$  are parameters of the fit. This functional form was motivated by combining the usual finite size scaling assumption that  $\xi = L$  with the Kosterlitz-Thouless expression for the critical behavior of the correlation length  $\xi$  [26],

$$\xi_\infty(K) \sim e^{bt^{-\nu}} \quad (11)$$

where  $t$  is the reduced temperature and  $\nu = 1/2$ . For this fit we found  $K_c = 1.120(1)$  and  $a = 2.49(4)$  with  $\chi^2 = 3.9$ ,  $\chi^2/d.o.f. = 0.65$  and  $Q = 0.68$ . The choice of  $L \geq 80$  was a compromise between keeping the error in  $K_c$  small and the confidence level  $Q$  large. The result for  $K_c$  is in good agreement with some of the recent results from the literature as shown in Table VII. Although the fit is good, the result for  $K_c$  should be viewed with caution because it is based on finite size scaling assumptions that do not necessarily hold for the IC ensemble.

Figure 4 shows the standard deviation  $\sigma_{1/\tilde{\kappa}}$  of  $1/\tilde{\kappa}$  as a function of  $1/\log^2(L)$ . Unlike the situation in three-dimensions, it is not clear that  $\sigma_{1/\tilde{\kappa}}$  vanishes as  $L \rightarrow \infty$ . If the finite size scaling behavior of the IC ensemble is of the “essential singularity” type observed in the canonical ensemble then a reasonable hypothesis is that  $\sigma_{1/\tilde{\kappa}} \sim (\log L)^{-q}$ . A naive extrapolation suggests  $\sigma_{1/\tilde{\kappa}}$  approaches a finite value near 0.11 but a slowly decreasing function cannot be ruled out. In the previous section we discussed reasons for the broad distribution of the temperature estimator. Simulations with  $L \gg 2000$  would be needed to determine whether or not  $\sigma_{1/\tilde{\kappa}}$  vanishes as  $L \rightarrow \infty$ .

### C. Magnetic Exponents

The average mass  $M$  of the spanning cluster is proportional to the magnetization of the system so that the magnetic exponents can be obtained from the fractal dimension of the

spanning cluster, defined by  $M \sim L^D$ . The critical exponent  $\eta$  is related to  $D$  via,

$$\eta = 2 + d - 2D. \quad (12)$$

Figure 5 shows a log-log plot of  $M$  vs.  $L$  for the three-dimensional  $XY$  model. A linear fit yields  $\eta(3D) = 0.037(2)$  with  $\chi^2 = 2.1$ ,  $\chi^2/d.o.f. = 0.35$  and the confidence level  $Q = 0.9$ . The smallest value of  $L$  included in the fit is  $L_{min} = 50$ . Figure 6 shows values of  $\eta$  obtained from fits with smallest linear size  $L_{min}$ . The value of  $\eta$  has an upward trend up to  $L_{min} = 40$  and then is constant for larger values of  $L_{min}$ . The value of  $L_{min}$  for the reported results was chosen such that the statistical error is minimal for a reasonably large  $Q$  and the value of  $\eta$  is well into the region of constant values. The plot on Fig. 6 also shows an upward trend for the two last values of  $L_{min}$ . Table VI shows some recent results for the three-dimensional  $XY$  model. Our result for  $\eta$  agrees with recently published values.

Figure 7 shows a log-log plot of  $M$  vs.  $L$  for the two-dimensional  $XY$  model. A linear fit to the data yields  $\eta(2D) = 0.251(5)$  which is in good agreement with the theoretical value for the Kosterlitz-Thouless transition  $\eta_{KT} = 0.25$ . The smallest value of  $L$  included in the fit is  $L_{min} = 480$  and  $\chi^2 = 2.84$ ,  $\chi^2/d.o.f. = 0.94$  and  $Q = 0.41$ . The value of  $L_{min}$  was chosen such that the statistical error is minimal for a reasonably large  $Q$ .

#### D. Dynamics of the invaded cluster algorithm

The *autocorrelation function* for a time dependent variable  $A(t)$  is defined as:

$$\Gamma_A(t) = \frac{\langle (A(0) - \langle A \rangle)(A(t) - \langle A \rangle) \rangle}{\langle (A(0) - \langle A \rangle)^2 \rangle} \quad (13)$$

The *integrated autocorrelation time* is defined by

$$\tau_A = \frac{1}{2} + \lim_{w \rightarrow \infty} \sum_{t=1}^w \Gamma_A(t). \quad (14)$$

The integrated autocorrelation time for  $A$  is interpreted as the time needed to obtain statistically independent measurements of  $A$ . As a result, the statistical error in measuring  $A$  in a MC simulation is proportional to  $(\tau_A/N)^{1/2}$  where  $N$  is the number of MC steps.

We measured the autocorrelation functions and the corresponding integrated autocorrelation times for the magnetization  $M$  and the critical coupling estimator  $\tilde{\kappa}$ . When calculating the integrated autocorrelation time it is necessary to choose a finite cut-off for  $w$  in the sum

in Eq. (14). We used  $w = 100$ , a value much longer than the integrated autocorrelation times obtained below. Figure 8 shows the autocorrelation function versus time for the inverse critical temperature of the three-dimensional  $XY$  model. Figure 9 shows the same plot for the two-dimensional case. Note the negative overshoot of the correlation functions for time of one MC step. This is due to the presence of a negative feedback mechanism in the IC algorithm. Consecutive temperature estimators for the spin configurations are anti-correlated.

Table V shows the integrated autocorrelation times for the mass of spanning cluster  $\tau_M$  and the inverse temperature  $\tau_{K_c}$  as a function of the linear size of the system  $L$  in the three-dimensional  $XY$  model. Table IV shows the same data for the two-dimensional case. These data show that the autocorrelation times for  $M$  and  $\tilde{\kappa}$  are independent of the system size. This behavior was also observed for IC dynamics for Ising-Potts models [17, 19, 27] and gives the impression that the IC algorithm does not have any critical slowing down. However, as shown by Moriarty, Machta and Chayes[19] for Ising-Potts models, observables defined on scales intermediate between the lattice spacing and system size have relaxation times that diverge with system size so that the dynamic exponent for the algorithm is greater than zero. Nonetheless, the small values of  $\tau_{\tilde{\kappa}}$  and  $\tau_M$  mean that relatively few MC steps are needed to obtain good statistics for  $\tilde{\kappa}$  and  $M$ .

#### IV. THE SOFT SPIN $O(2)$ MODEL

The values of  $\eta$  for the three-dimensional  $XY$  universality class vary significantly in the literature. Table VI shows some recent results for  $\eta$ . Possible reason this discrepancy in the literature is the presence of finite size scaling correction in the fit of  $M$  vs.  $L$ . Hasenbusch and Török [6] and Campostrini *et al.*[7] studied a  $\phi^4$  *soft spin* model defined by the Hamiltonian:

$$H/T = -J/T \sum_{\langle i,j \rangle} \vec{\phi}_i \cdot \vec{\phi}_j + \sum_i \phi_i^2 + \lambda \sum_i (\phi_i^2 - 1)^2 \quad (15)$$

where  $T$  is the temperature,  $J$  interaction constant and  $\lambda$  a “softness” parameter. The vectors  $\vec{\phi}$  can have any value of the modulus  $|\vec{\phi}|$ . The  $XY$  model is obtained as a special case for  $\lambda = \infty$ . This model is in the same universality class as the three-dimensional  $XY$  model. Hasenbusch and Török showed that finite size corrections in the canonical ensemble are minimized near  $\lambda = 2.0$ .

We implemented the IC algorithm for the soft spin model. Following Refs. [28] and [6] we used the IC algorithm to update the orientation of the vectors  $\vec{\phi}$  and the Metropolis algorithm to update the modulus. The IC part of the combined algorithm is described in Sec. 2. The only difference is that the modulus of the spins does not necessarily have the value of  $|\vec{\phi}| = 1$ . Since the IC algorithm performs only reflections, the modulus of the spins remains the same after the IC sweep. After every IC step, the algorithm performs an update of both the modulus and the orientation of the spins using the Metropolis algorithm as follows. New values of the two spin components are proposed:

$$\phi_x' = \phi_x - 2(p_x - 0.5)$$

$$\phi_y' = \phi_y - 2(p_y - 0.5)$$

where  $p_x$  and  $p_y$  are random numbers from the interval  $[0, 1)$ . The update is accepted with the probability

$$P = \min[1, \exp(H/T - H'/T)]$$

where  $T$  is obtained from the output of the previous IC step. The temperature will therefore be different for every Metropolis update. However, as is the case for the three-dimensional  $XY$  model, these temperature fluctuations tend toward zero as  $L \rightarrow \infty$ . In the limit of very large system size the Metropolis subroutine updates the system at a fixed temperature. The Metropolis subroutine preserves the negative feedback mechanism of the IC algorithm. If the temperature of the system is low, the Metropolis algorithm will tend to make the modulus of the spins larger. With larger spin modulus the IC algorithm will give a higher temperature as an outcome. The same holds if we start with high temperature. The Metropolis algorithm will make the modulus of the spins smaller and consequently the IC algorithm will lower the temperature.

In our simulations of the soft spin model we used  $\lambda = 2.0$ . The maximum linear size of the system was  $L = 120$  and each run consisted of 10000 MC steps. Figure 10 shows the average critical coupling  $\langle \tilde{\kappa} \rangle$  vs.  $1/L$ . A fit to the function  $\langle \tilde{\kappa} \rangle = K_c/(1 + aL^{-p})$  yields  $K_c(\lambda = 2.0) = 0.5100(1)$ ,  $a = -0.9(4)$  and  $p = 1.3(1)$ . The smallest size included in the fit is  $L = 30$  and  $\chi^2 = 10.0$ ,  $\chi^2/d.o.f. = 1.4$  and  $Q = 0.18$ . This value of  $K_c$  is in agreement with the value reported by Hasenbusch and Török [6]  $K_c = 0.5099049(6)$ . Figure 11 shows a log-log plot of  $M$  vs.  $L$ . The resulting value for  $\eta$ ,  $\eta(\lambda = 2.0) = 0.042(8)$  (with  $\chi^2 = 5.8$ ,

$\chi^2/d.o.f. = 0.98$  and  $Q = 0.43$ ) is in agreement with their result  $\eta = 0.0381(2)$ . A recent work by Campostrini *et. al.*[7] yielded  $\eta = 0.0380(4)$ .

## V. CONCLUSIONS

In this paper we have introduced and applied an invaded cluster algorithm for the two and three-dimensional  $XY$  models and a related three-dimensional soft spin model. This work extends the range of validity of the invaded cluster method to include continuous spins and systems where the phase transition is of the Kosterlitz-Thouless type. Our results for critical temperatures and magnetic exponents are in reasonable agreement with recent values in the literature. The invaded cluster algorithm is very efficient for  $XY$  systems, showing no critical slowing for estimators of the critical temperature and the magnetization and yielding highly accurate values of the magnetic exponent with relatively little computational effort.

## VI. ACKNOWLEDGMENTS

The authors would like to thank Nikolay Prokof'ev for useful discussions. This work was supported in part by NSF grant DMR 9978233.

- 
- [1] J. M. Kosterlitz and D. J. Thouless, *J. Phys. C* **6**, 1181 (1973).
  - [2] P. Butera and M. Comi, *Phys. Rev. B* **56**, 8212 (1997).
  - [3] R. Guida and J. Zinn-Justin, *J. Phys. A: Math. Gen.* **31**, 8103 (1998).
  - [4] W. Janke, *Phys. Lett. A* **148**, 306 (1990).
  - [5] A. P. Gottlob and M. Hasenbusch, *Physica A* **201**, 593 (1993).
  - [6] M. Hasenbusch and T. Török, *J. Phys. A: Math. Gen.* **32**, 6361 (1999).
  - [7] M. Campostrini, M. Hasenbusch, A. Pelissetto, P. Rossi, and E. Vicari, *Critical behavior of the three-dimensional XY universality class* (2000), cond-mat/0010360.
  - [8] J. A. Lipa, D. R. Swanson, J. Nissen, T. C. P. Chui, and U. E. Israelson, *Phys. Rev. Lett.* **76**, 944 (1996).
  - [9] L. S. Goldner, N. Mulders, and G. Ahlers, *J. Low Temp. Phys.* **93**, 131 (1993).
  - [10] D. R. Swanson, T. C. P. Chui, and J. A. Lipa, *Phys. Rev. B* **46**, 9043 (1992).

- [11] U. Wolff, Phys. Rev. Lett. **62**, 361 (1989).
- [12] R. H. Swendsen and J.-S. Wang, Phys. Rev. Lett. **58**, 86 (1987).
- [13] M. E. J. Newman and G. T. Barkema, *Monte Carlo Methods in Statistical Physics* (Oxford, Oxford, 1999).
- [14] D. Kandel and E. Domany, Phys. Rev. B **43**, 8539 (1991).
- [15] L. Chayes and J. Machta, Physica A **239**, 542 (1997).
- [16] L. Chayes and J. Machta, Physica A **254**, 477 (1998).
- [17] J. Machta, Y. S. Choi, A. Lucke, T. Schweizer, and L. V. Chayes, Phys. Rev. Lett. **75**, 2792 (1995).
- [18] J. Machta, Y. S. Choi, A. Lucke, T. Schweizer, and L. M. Chayes, Phys. Rev. E **54**, 1332 (1996).
- [19] K. Moriarty, J. Machta, and L. Y. Chayes, Phys. Rev. E **59**, 1425 (1999).
- [20] T. B. Liverpool and S. C. Glotzer, Phys. Rev. E **53**, R4255 (1996).
- [21] G. Franzese, V. Cataudella, and C. A., Phys. Rev. E **57**, 88 (1998).
- [22] G. Johnson, H. Gould, J. Machta, and L. K. Chayes, Phys. Rev. Lett. **79**, 2612 (1997).
- [23] A. Coniglio and W. Klein, J. Phys. A: Math. Gen. **13**, 2775 (1980).
- [24] M. Aizenman, J. T. Chayes, L. Chayes, and C. M. Newman, J. Stat. Phys. **50**, 1 (1988).
- [25] L. Chayes, Comm. Math. Phys. **197**, 623 (1998).
- [26] J. M. Kosterlitz, J. Phys. C **7**, 1046 (1974).
- [27] Y. S. Choi, J. Machta, P. Tamayo, and L. Chayes, Int. J. Mod. Phys. C **10**, 1 (1999).
- [28] R. Brower and P. Tamayo, Phys. Rev. Lett. **62**, 1087 (1989).
- [29] H. G. Ballesteros, L. A. Fenández, V. Martín-Mayor, and A. Muñoz Sudupe, Phys. Lett. B **387**, 125 (1996).
- [30] F. Jasch and H. Kleinert, J. Math. Phys. **42**, 52 (2001).
- [31] M. Krech and D. P. Landau, Phys. Rev. B **60**, 3375 (1999).
- [32] B. Zheng, M. Schultz, and S. Trimper, Phys. Rev. E **59**, R1351 (1999).
- [33] R. Kena and A. C. Irving, Nucl. Phys. B **485**, 583 (1997).
- [34] M. Hasenbusch and K. Pinn, J. Phys. A: Math. Gen. **30**, 63 (1997).
- [35] J. K. Kim, Phys. Lett. A **223**, 261 (1996).
- [36] P. Olsson, Phys. Rev. B **52**, 4526 (1995).

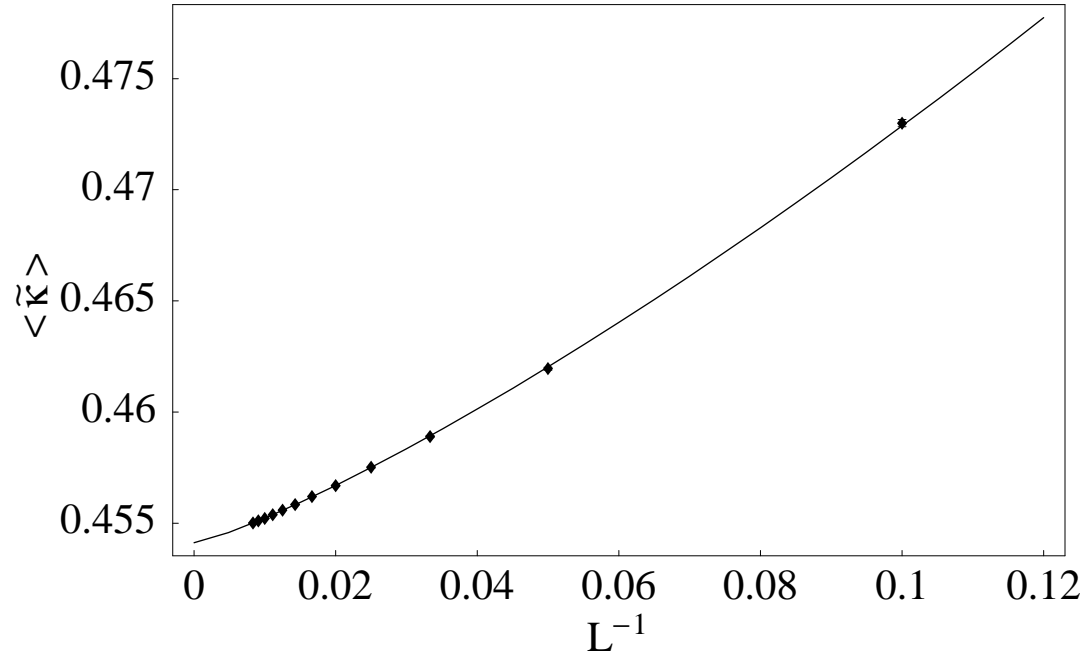


FIG. 1: Critical coupling  $\langle \tilde{\kappa} \rangle$  vs.  $1/L$  for the three-dimensional  $XY$  model. The solid line is a fit to the data as described in the text.

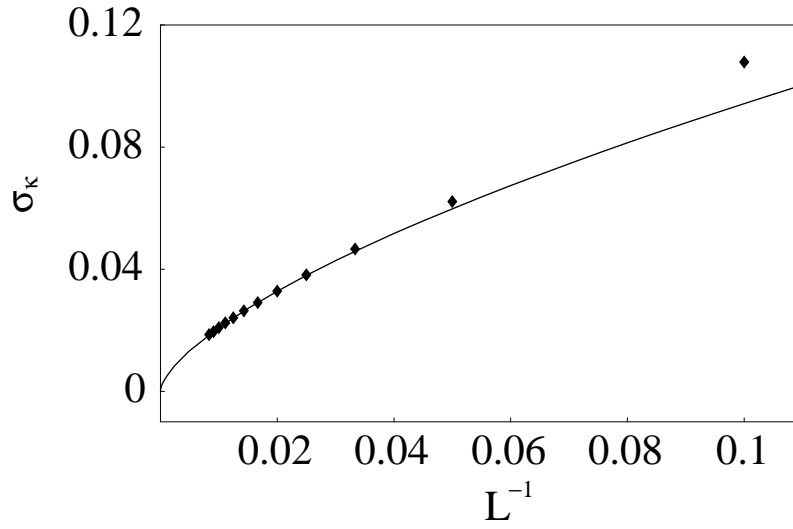


FIG. 2: Standard deviation of the critical coupling  $\sigma_{\tilde{\kappa}}$  vs.  $1/L$  for three-dimensional XY model. The solid line is a fit to the data as described in the text.



L	$\sigma_{\tilde{\kappa}}$	$\tilde{\kappa}$	M
10	0.1079(2)	0.4730(2)	236.2(2)
20	0.0621(1)	0.46195(7)	1334(1)
30	0.04658(8)	0.45890(5)	3662(3)
40	0.03810(7)	0.45751(3)	7480(4)
50	0.03281(6)	0.45668(2)	13038(10)
60	0.02904(5)	0.45620(2)	20474(18)
70	0.02635(4)	0.45584(2)	30052(25)
80	0.02409(4)	0.45558(1)	41820(36)
90	0.02240(4)	0.45538(1)	56047(46)
100	0.02080(4)	0.45521(1)	72824(64)
110	0.01957(3)	0.45511(1)	92197(80)
120	0.01854(3)	0.455006(9)	114374(96)

TABLE I: Numerical data for the three-dimensional  $XY$  model.

L	$\sigma_{\tilde{T}}$	$\tilde{\kappa} \equiv 1/\tilde{T}$	M
10	0.44(5)	0.788(2)	55.5(1)
20	0.32(5)	0.891(1)	200.6(5)
40	0.25(5)	0.953(1)	717(2)
80	0.22(5)	0.9936(7)	2631(6)
160	0.19(5)	1.0212(8)	9543(24)
240	0.19(5)	1.0350(8)	20151(50)
320	0.18(5)	1.0410(8)	34779(86)
480	0.17(5)	1.0519(9)	74083(186)
640	0.16(5)	1.0571(7)	126798(311)
800	0.17(5)	1.0605(7)	192100(490)
1000	0.16(5)	1.0643(6)	293519(756)
2000	0.15(5)	1.0742(7)	1073907(2800)

TABLE II: Numerical data for the two-dimensional  $XY$  model.

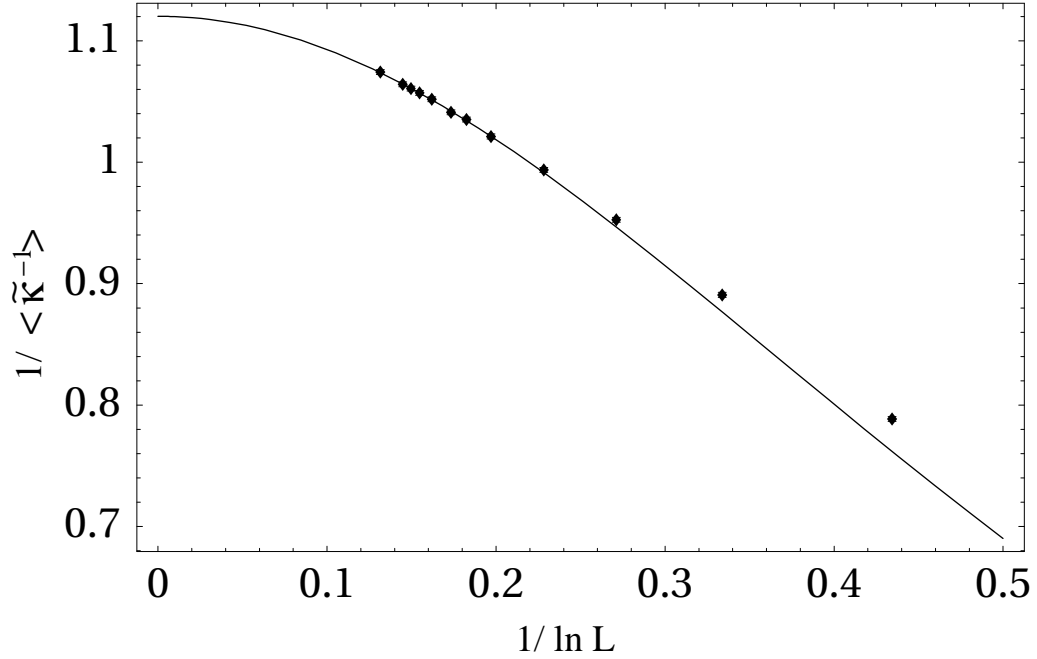


FIG. 3: Critical coupling  $1/\langle\tilde{\kappa}^{-1}\rangle$  vs.  $1/\ln(L)$  for two-dimensional  $XY$  model. The solid line is a fit to the data as described in the text.

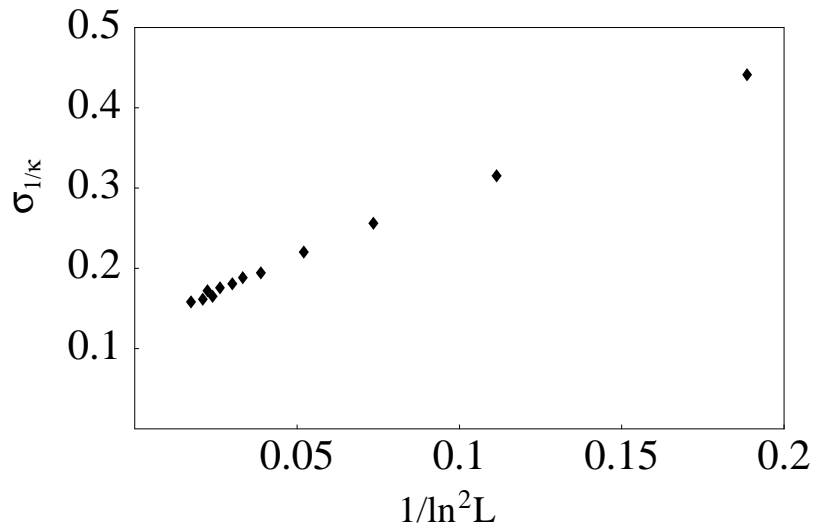


FIG. 4: Standard deviation of the critical coupling  $\sigma_{1/\kappa}$  vs.  $1/\ln^2(L)$  for two-dimensional  $XY$  model.

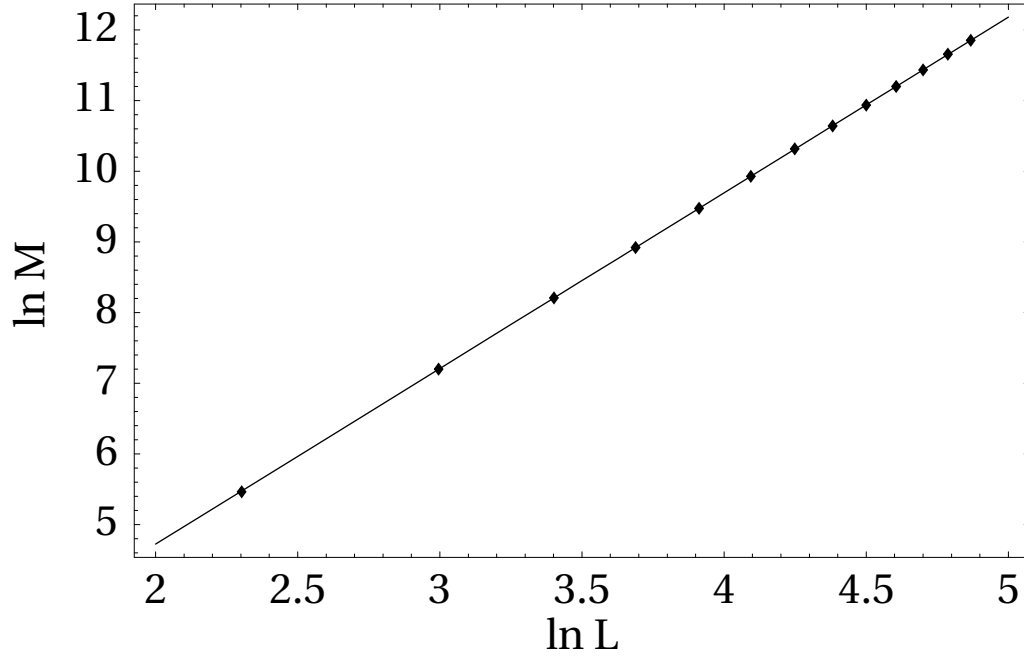


FIG. 5: Mass of the spanning cluster  $\ln M$  vs.  $\ln L$  for the three-dimensional  $XY$  model. The solid line is a linear fit.

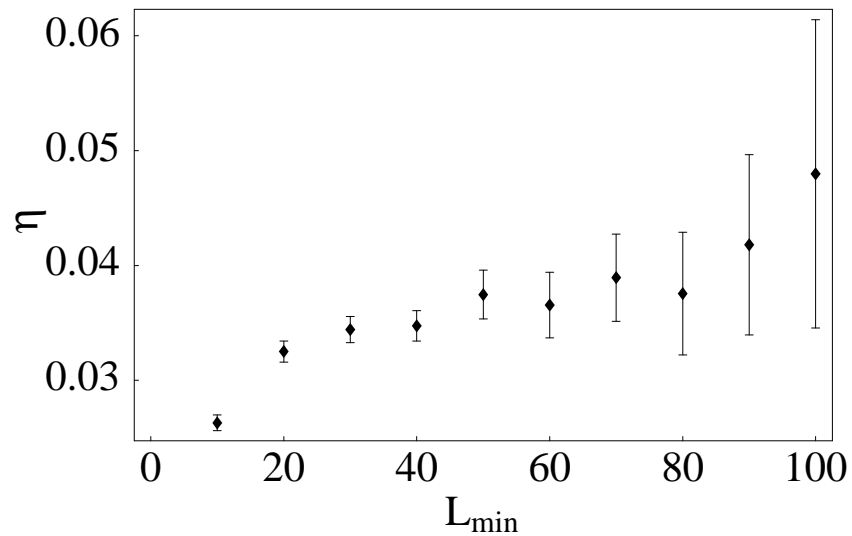


FIG. 6: The critical exponent  $\eta$  for the three-dimensional  $XY$  model vs. minimum system size  $L_{min}$  included in the fit of the data. The maximum system size in the fit is  $L_{max} = 120$ .

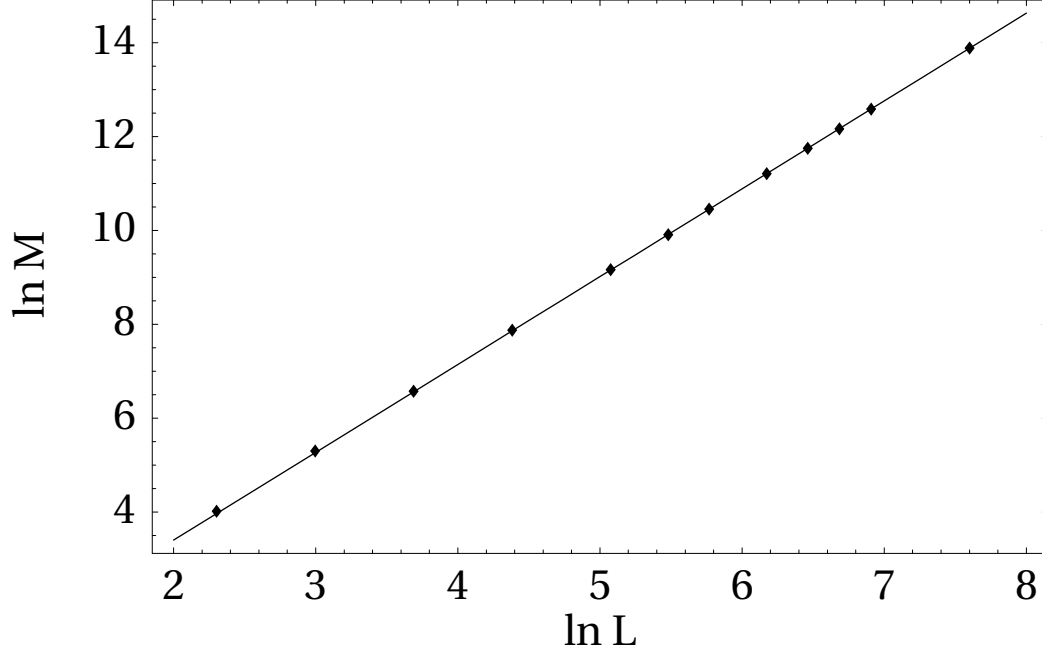


FIG. 7: Mass of the spanning cluster  $\ln M$  vs.  $\ln L$  for two-dimensional  $XY$  model. The solid line is a linear fit.

$L$	$\sigma_{\tilde{\kappa}}$	$\tilde{\kappa}$	$M$
10	0.151(1)	0.562(1)	229(1)
20	0.0906(6)	0.5486(9)	1288(4)
30	0.0652(5)	0.5160(7)	3540(10)
40	0.0498(3)	0.5139(5)	7270(20)
50	0.0437(3)	0.5151(4)	12691(40)
60	0.0382(3)	0.5123(4)	19988(70)
70	0.0377(2)	0.5120(4)	29404(100)
80	0.0320(2)	0.5116(3)	40846(140)
90	0.0320(2)	0.5115(3)	54384(200)
100	0.0300(2)	0.5113(4)	70784(240)
110	0.0282(2)	0.5111(3)	89484(300)
120	0.0266(2)	0.5112(3)	111851(400)

TABLE III: Numerical data for the three-dimensional soft spin model with  $\lambda = 2.0$ .

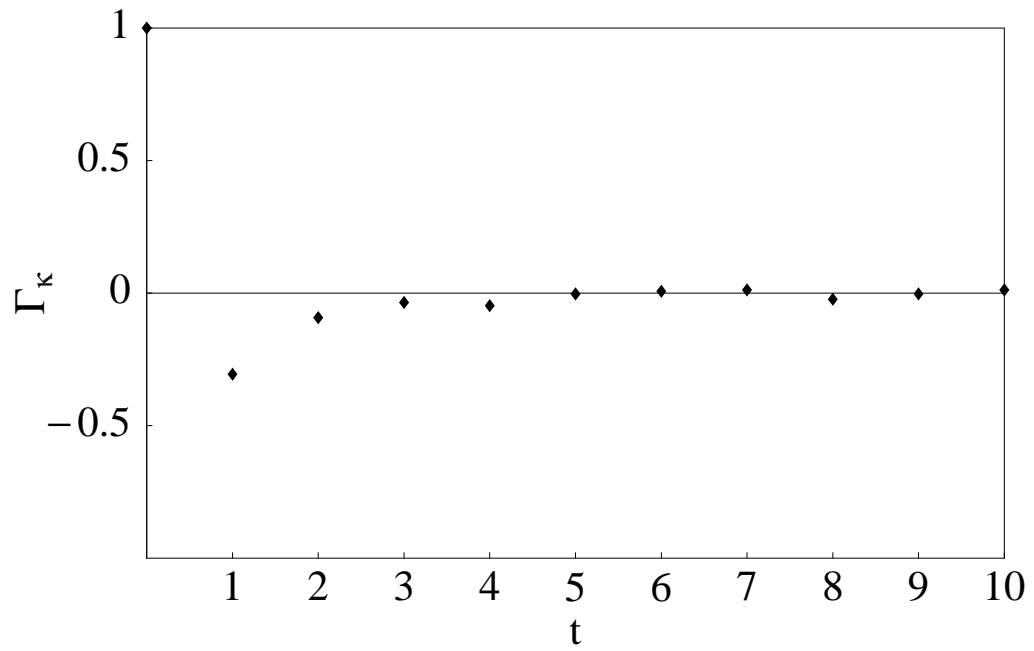


FIG. 8: The autocorrelation function of the critical coupling  $\Gamma_{\tilde{\kappa}}$  vs. Monte Carlo time for the three-dimensional  $XY$  model. The system size is  $L=100$ .

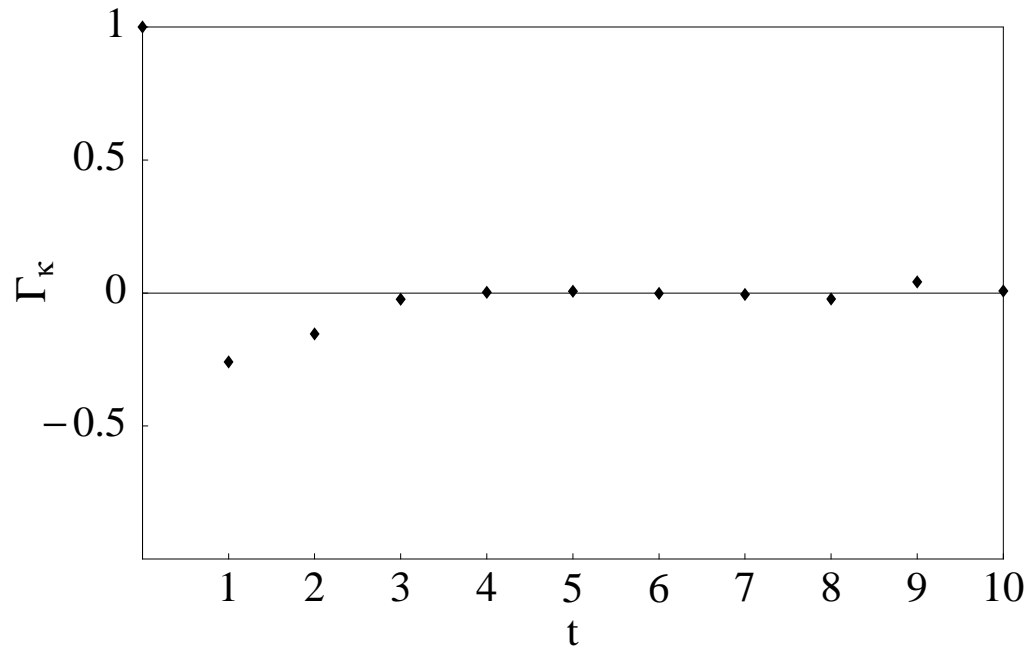


FIG. 9: The autocorrelation function for the Kosterlitz-Thouless temperature estimator  $\Gamma_{\tilde{\kappa}}$  vs. Monte Carlo time for the two-dimensional  $XY$  model. The system size is  $L=1000$ .

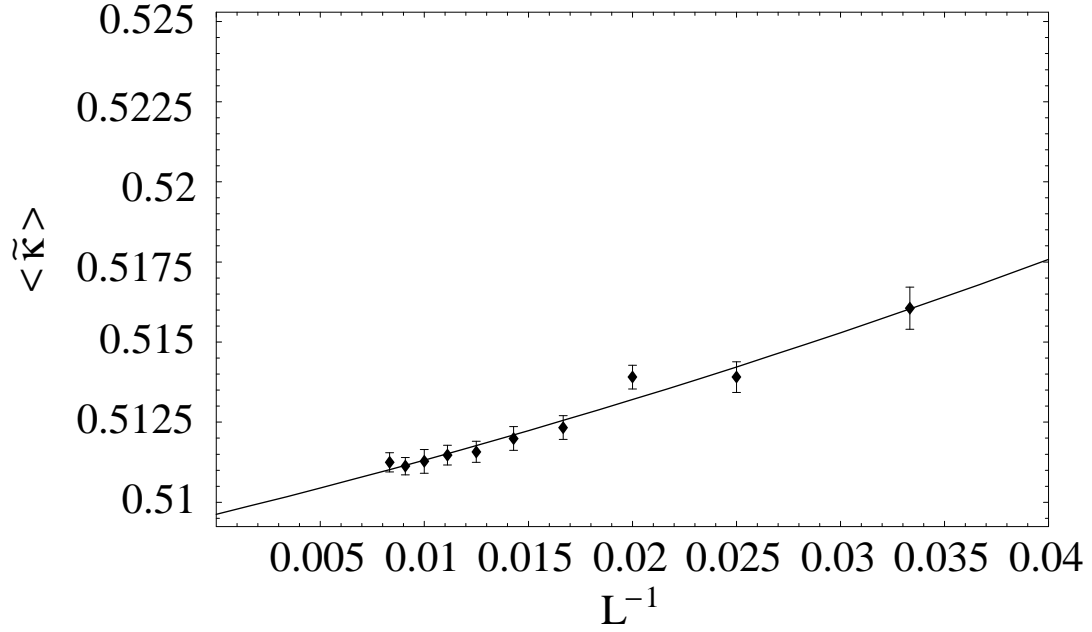


FIG. 10: Critical coupling  $\langle \tilde{\kappa} \rangle$  vs.  $1/L$  for the three-dimensional soft spin model. The solid line is a fit to the data as described in the text.

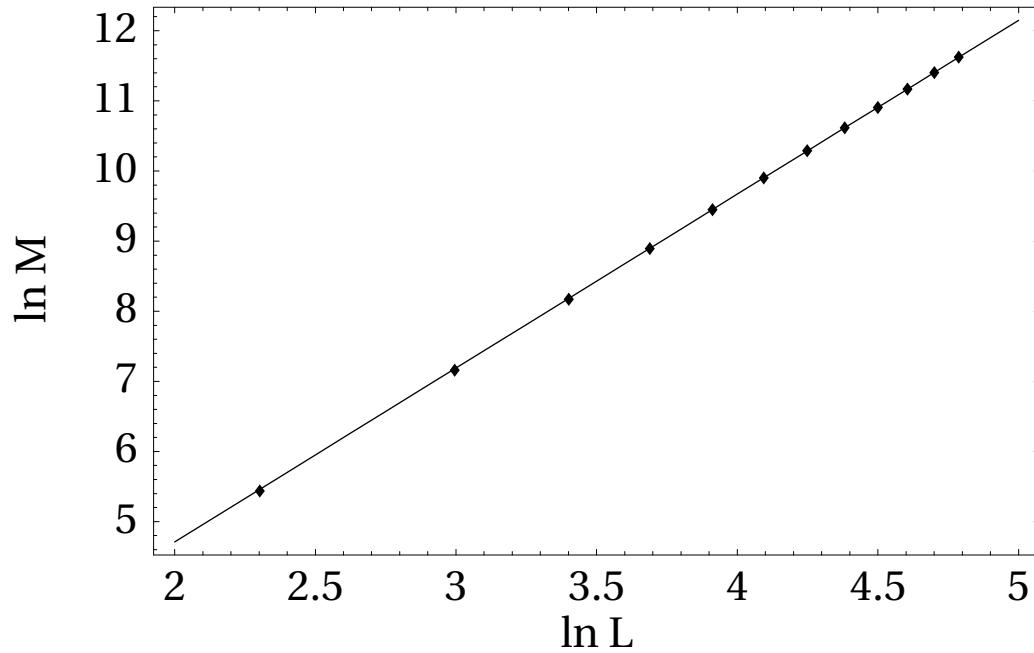


FIG. 11: Mass of the spanning cluster  $\ln M$  vs.  $\ln L$  for three-dimensional soft spin model. The solid line is a linear fit.

L	$\tau_{\tilde{\kappa}}$	$\tau_M$
10	0.195	0.50
20	0.129	0.56
30	0.045	0.52
40	0.052	0.52
50	0.045	0.51
60	0.028	0.50
70	0.025	0.50
80	0.021	0.49
90	0.028	0.50
100	0.029	0.58
110	0.010	0.52
120	0.032	0.61

TABLE IV: Autocorrelation times for critical coupling  $\tau_{\tilde{\kappa}}$  and magnetization  $\tau_M$  for the three-dimensional  $XY$  model.



L	$\tau_{\tilde{\kappa}}$	$\tau_M$
10	0.273	0.73
20	0.144	0.95
40	0.107	0.57
80	0.077	0.71
160	0.095	0.88
240	0.061	1.15
320	0.073	0.80
480	0.097	0.99
640	0.071	1.07
800	0.082	0.82
1000	0.060	0.60
2000	0.073	0.64

TABLE V: Autocorrelation times for critical coupling  $\tau_{\tilde{\kappa}}$  and magnetization  $\tau_M$  for the two-dimensional  $XY$  model.

Ref.	method	$K_c$ ( $XY$ )	$\eta$
This work ( $XY$ )	MC	0.45412(2)	0.037(2)
This work (soft spin)	MC	-	0.042(8)
[4]	MC	0.45408(8)	0.036(14)
[7]	MC+HT	-	0.0380(4)
[29]	MC	0.454165(4)	0.042(2)
[6]	MC	-	0.0381(2)
[5]	MC	0.45420(2)	0.024(6)
[3]	FT	-	0.038(6)
[2]	HT	0.45419(3)	0.039(7)
[30]	FT	-	0.0349(8)
[31]	MC	-	0.035(5)

TABLE VI: A summary of recent estimates of the critical coupling for the three-dimensional  $XY$  model and the exponent  $\eta$  for the three-dimensional  $O(2)$  universality class.

Ref.	method	$K_c$	$\eta$
This work	MC	1.120(1)	0.251(5)
[32]	MC	1.118	0.238(4)
[33]	MC	1.113(6)	-
[34]	MC	1.1199(1)	0.233(3)
[35]	MC	1.106(5)	-
[36]	MC	1.1209(1)	-

TABLE VII: A summary of recent estimates of the critical coupling and the exponent  $\eta$  for two-dimensional  $XY$  model on a simple cubic lattice. According to the Kosterlitz-Thouless theory  $\eta = 1/4$ .